JOURNAL OF SOLID STATE CHEMISTRY 46, 234–244 (1983)

The Crystal Structures and Magnetic Properties of Ba_2LaRuO_6 and Ca_2LaRuO_6

P. D. BATTLE,* J. B. GOODENOUGH, AND R. PRICE

Inorganic Chemistry Laboratory, South Parks Road, Oxford, OX1 3QR, England

Received July 22, 1982

Profile analysis of high-resolution, powder neutron-diffraction data was used to refine the previously reported structures of the ordered, distorted perovskites Ba_2LaRuO_6 and Ca_2LaRuO_6. Low-temperature neutron diffraction experiments showed that, at 2K, the former is a Type IIIa antiferromagnet while the latter is Type I. Both compounds have an ordered magnetic moment of $\mu_{Ru} \simeq 1.95\mu_B$ per Ru^{5+} ion. The Néel temperature of Ba_2LaRuO_6 was determined to be 29.5K, and the covalent mixing between the ruthenium and nearest-neighbor anions is described by $A_\pi^2 = 8.2 \pm 1\%$ for Ba_2LaRuO_6 and $8.6 \pm 1\%$ for Ca_2LaRuO_6. The ionic radius of a Ru^{5+} ion is 0.56 Å. These data are consistently interpreted within the framework of a strongly correlated, half-filled π^* band. Extension of this interpretation to the magnetic data for the perovskites $CaRuO_3$ and $SrRuO_3$ leads to a fundamental theoretical prediction.

Introduction

Donohue and McCann (*1*) first described the preparation of Ba_2LaRuO_6 in a report on automobile emission-control catalysts. X-Ray powder-diffraction measurements indicated a simple-cubic perovskite structure with a unit cell parameter $a = 4.273$ Å, and chemical analysis established that the ruthenium is in the pentavalent state. A subsequent X-ray study by Greatrex *et al.* (*2*) showed that the *B*-site cations are ordered, thus causing a doubling of the cubic unit cell. The first preparation and characterization of Ca_2LaRuO_6 was performed by Greatrex *et al.* (*2*), who indexed their X-ray powder-diffraction data using an orthorhombic, perovskite-like unit cell ($a = 5.817$, $b = 5.600$, $c = 8.038$ Å) with ordered *B*-site cations (Fig. 1). They assumed that the *B* sites were occupied by lanthanum and ruthenium in both materials, thus leaving the *A* sites occupied by the alkaline earth. A low-resolution neutron-diffraction experiment (*3*) has subsequently shown this assumption to be false in the case of Ca_2LaRuO_6, where the *B* sites are occupied by ruthenium and half of the calcium, the *A* sites containing a disordered array of lanthanum and the remaining calcium. Furthermore, the neutron work showed that Greatrex *et al.* overestimated the symmetry of both Ba_2LaRuO_6 and Ca_2LaRuO_6. Unfortunately, the present high-resolution neutron study has revealed that the symmetry was incorrectly assigned once again in the earlier work, and the atomic coordinates given in that work are superseded by those presented below.

*Author to whom correspondence should be addressed.

0022-4596/83/020234-11$03.00/0

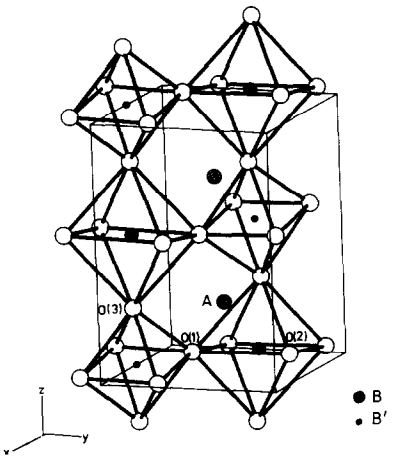

FIG. 1. The unit cell for the ordered, distorted perovskite $A_2BB'O_6$ showing the crystallographically distinct atoms.

Greatrex *et al.* also investigated Ca_2LaRuO_6 and Ba_2LaRuO_6 by ^{99}Ru Mössbauer spectroscopy. The isomer shifts they observed confirm the presence of Ru^{5+} in both compounds. Furthermore, their low-temperature Mössbauer experiments showed that both materials are magnetically ordered at 4.2K. Magnetic ordering of highly oxidized cations from the second transition series is quite unusual, and these perovskites offer a rare opportunity to study the magnetic behavior of a $4d^3$ electron system. We therefore carried out low-temperature, powder neutron-diffraction experiments to determine the type of magnetic ordering that occurs and the magnitude of the ordered magnetic moment. We also determined the Néel temperature of Ba_2LaRuO_6 to complete the set of susceptibility data presented by Greatrex *et al.*

Experimental

The samples used for the high-resolution neutron-diffraction experiments were the same ones used in the earlier low-resolution study (*3*). The neutron diffraction profiles of Ba_2LaRuO_6 and Ca_2LaRuO_6 were recorded at room temperature by using the instrument D1a at ILL Grenoble operating at a wavelength of 1.909 Å and a monitor count of 4.5×10^4 (Ca) or 3.0×10^4 (Ba) neutrons. The samples were contained in 12-mm-diameter vanadium cans mounted in an aluminum-tailed cryostat. Further experiments were performed at 2K with monitor counts of 4.5×10^4 (Ca) and 5.0×10^4 (Ba) neutrons. In all cases, the diffractometer counters were moved with a 2θ step size of 0.05°.

The magnetic susceptibility of Ba_2LaRuO_6 was measured in the temperature range 4.2–90K with an Oxford Instruments Faraday balance. A magnetic field of 38.1 kG was used with a field gradient of 121.1 G cm^{-1}.

Results

1. Neutron Diffraction

The neutron-diffraction patterns were all analyzed by the profile-analysis technique (*4*). The data on Ca_2LaRuO_6 were contaminated by scattering from aluminum in the cryostat, and the effected regions of the profiles have been excluded from the structure refinements, as have the low-angle, asymmetric peaks (*5*). The following scattering lengths were used: $b_{Ba} = 0.52$, $b_{Ca} = 0.47$, $b_{La} = 0.83$, $b_{Ru} = 0.73$ and $b_O = 0.58 \times 10^{-14}$ m (*6*).

(*a*) *Room-temperature results.* Initially we attempted to fit the data collected on Ba_2LaRuO_6 at room temperature to the monoclinic structure proposed in the earlier work (*3*). It was immediately apparent that the low-resolution data had been analyzed in an incorrect space group ($P2_1/n$), and it became clear that Ba_2LaRuO_6 is actually triclinic at room temperature with space group $P\bar{1}$. However, to facilitate easy comparison with other perovskite structures, including Ca_2LaRuO_6, we shall work with the space group $I\bar{1}$, and hence with a unit

cell (Fig. 1) twice the volume of the primitive cell. Least-squares refinement of twelve positional parameters, four isotropic temperature factors, and the usual profile parameters gave a weighted profile R factor of 9.5%. The cell parameters refined to the following values:

$$a = 6.0299(6),\ b = 6.0587(6),\ c = 8.5371(9)\ \text{Å},$$
$$\alpha = 89.86(1),\ \beta = 90.33(1),\ \gamma = 90.03(1)°.$$

Here and throughout this paper the number in brackets is the estimated standard deviation in the last figure. The final atomic coordinates and temperature factors are listed in Table I, and the bond lengths and bond angles are given in Table II. The observed, calculated, and difference profiles are plotted in Fig. 2. This structure obviously possesses a high degree of pseudosymmetry, and the atomic coordinates show that the symmetry is particularly close to monoclinic $I2/m$. However, refinements in that space group gave a lowest R factor of 11.9%, and this value was only achieved with some temperature factors negative.

Ca_2LaRuO_6 was previously (*3*) described as a triclinic structure, but the new data can be fitted to a monoclinic model. It appears that the starting parameters used in the earlier work were not close enough to the correct values for the least-squares program to converge on the true minimum. The atomic coordinates listed in Table III gave a weighted profile R factor of 8.0% in the monoclinic space group $P2_1/n$. Once again there were twelve atomic coordinates and four isotropic temperature factors to be refined. The bond lengths and bond angles are listed in Table IV, and the profiles are plotted in Fig. 3. The cell parameters refined to the following values:

$$a = 5.6180(1),\ b = 5.8366(1),\ c = 8.0677(1)\ \text{Å},\ \beta = 90.24(1)°.$$

(b) 2-K results. The low-temperature diffraction patterns of both samples showed peaks indicative of antiferromagnetic ordering. The patterns were otherwise very

TABLE I

ATOMIC POSITIONS AND ISOTROPIC TEMPERATURE FACTORS FOR Ba_2LaRuO_6 AT ROOM TEMPERATURE

Atom	x	y	z	B (Å²)
Ba	0.504(2)	0.506(2)	0.246(2)	0.85(5)
La	0	0.5	0	0.45(7)
Ru	0.5	0	0	0.50(8)
O(1)	0.274(3)	0.229(2)	−0.022(1)	1.12(4)
O(2)	0.261(2)	0.778(2)	0.025(1)	1.12(4)
O(3)	0.503(3)	0.037(2)	0.225(1)	1.12(4)

TABLE II

BOND LENGTHS (IN Å) AND BOND ANGLES (IN DEG.) FOR Ba_2LaRuO_6 AT ROOM TEMPERATURE

La–O(1)	2.34(2)	Ru–O(1)	1.95(2)
La–O(2)	2.31(2)	Ru–O(2)	1.99(2)
La–O(3)	2.36(2)	Ru–O(3)	1.93(2)

Ba–O(1)	Ba–O(2)	Ba–O(3)
3.16(3)	2.85(3)	2.85(3)
2.89(3)	3.23(3)	3.22(3)
2.83(3)	3.15(3)	3.08(3)
3.23(3)	2.89(3)	3.00(3)

O(1)–La–O(2)	92.1	O(1)–Ru–O(2)	90.7
O(1)–La–O(3)	91.5	O(1)–Ru–O(3)	90.9
O(2)–La–O(3)	90.9	O(2)–Ru–O(3)	91.4

Note. Estimated standard deviation in bond angles is 1°.

TABLE III

ATOMIC POSITIONS AND ISOTROPIC TEMPERATURE FACTORS FOR Ca_2LaRuO_6 AT ROOM TEMPERATURE

Atom	x	y	z	B (Å²)
Ca/La (*A* site)	0.5134(3)	0.5549(2)	0.2504(4)	0.88(3)
Ru	0.5	0	0	1.03(5)
Ca	0	0.5	0	0.06(7)
O(1)	0.2162(3)	0.1802(3)	−0.0498(3)	0.88(2)
O(2)	0.3238(4)	0.7205(3)	−0.0616(3)	0.88(2)
O(3)	0.3968(3)	−0.0414(3)	0.2290(3)	0.88(2)

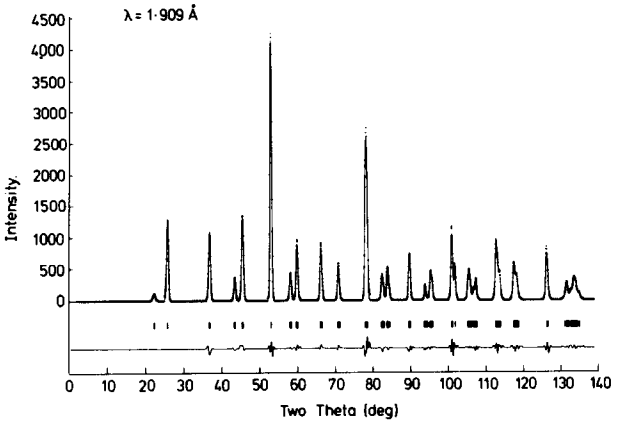

FIG. 2. The observed (dots), calculated (——), and difference profiles for Ba_2LaRuO_6 at room temperature. Reflection positions are marked. Data at $2\theta < 32°$ were not included in the profile analysis because of asymmetric peak shape.

similar to those collected at room temperature, except that the degree of distortion in the Ba_2LaRuO_6 lattice appeared to have increased on cooling. The strongest magnetic peak in each pattern occurred at $2\theta \sim 14°$ and was therefore too asymmetric in shape to be used in profile analysis (*5*). The remaining magnetic peaks were very weak, and we therefore chose to estimate the magnitude of the ordered magnetic moment by considering only the integrated intensity under the low-angle peak in each pattern. This method also removes the problem of fitting a form factor for the Ru^{5+} ion because at $2\theta = 14°$ it is a good approximation to assume a value of unity. In order to obtain a value for the magnetic moment, it is necessary to scale the intensity of the mag-

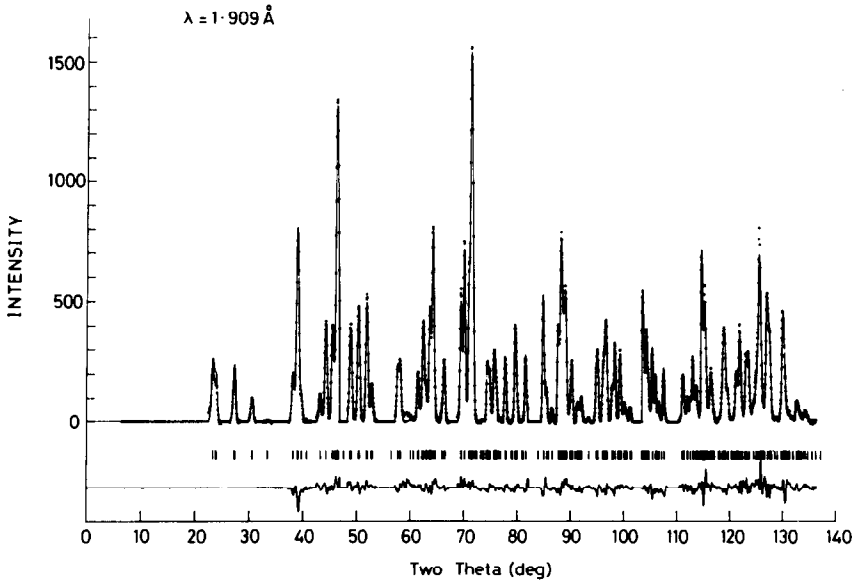

FIG. 3. The observed, calculated, and difference profiles for Ca_2LaRuO_6 at room temperature.

TABLE IV

BOND LENGTHS (IN Å) AND BOND ANGLES (IN DEG.) FOR Ca_2LaRuO_6 AT ROOM TEMPERATURE

Ca–O(1)	2.264(3)	Ru–O(1)	1.950(3)
Ca–O(2)	2.285(3)	Ru–O(2)	1.971(3)
Ca–O(3)	2.272(3)	Ru–O(3)	1.954(3)
O(1)–Ca–O(2)	90.1	O(1)–Ru–O(2)	90.9
O(1)–Ca–O(3)	93.0	O(1)–Ru–O(3)	90.9
O(2)–Ca–O(3)	94.0	O(2)–Ru–O(3)	90.8

Note. Estimated standard deviation in bond angles is 1°.

netic peak to that of a nuclear peak; we therefore refined the low-temperature crystal structures by profile analysis. The same atomic coordinates were varied as in the room-temperature calculations, but at 2K we used an overall isotropic temperature factor. The final unit-cell parameters are given in Table V, and the atomic coordinates in Tables VI and VII. The magnetic reflections in the diffraction pattern of Ba_2LaRuO_6 can be indexed on a pseudotetragonal unit cell with $a_m \sim \sqrt{2}a$, $b_m \sim \sqrt{2}b$, and $c_m = 2c$, the low-angle peak comprising the $\{101\}_{tet}$ reflections. This is characteristic of Type IIIa magnetic ordering (*7*) with the spin direction along c_m, as illustrated in Fig. 4. The ordered magnetic moment is then calculated as $1.96(10)\mu_B$ per Ru^{5+} ion. The magnetic reflections observed in the case of Ca_2LaRuO_6 can be indexed in a pseudoorthorhombic cell with $a_m \sim \sqrt{2}a$, $b_m \sim \sqrt{2}b$, and $c_m \sim c$. The low-angle magnetic peak is then the (100) reflection, indicating that this material shows Type I magnetic ordering with a spin direction perpendicular to a_m, as illustrated in Fig. 5.

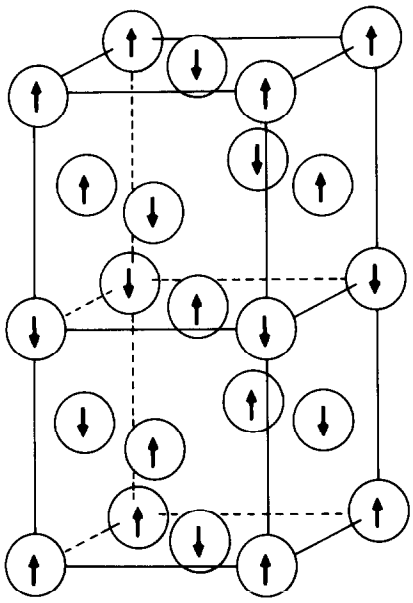

FIG. 4. The Type IIIa magnetic unit cell for Ba_2LaRuO_6. Only ruthenium ions are shown.

The magnetic moment is calculated to be $1.92(10)\mu_B$ per Ru^{5+} ion.

2. Magnetic Susceptibility

The low-temperature magnetic susceptibility of Ba_2LaRuO_6 is plotted in Fig. 6. The Néel temperature is 29.5K, and there is some evidence of a spin–flop transition below 10K. This is not unreasonable in view of the strength of magnetic field used.

Discussion

1. Crystal Structures

The high-resolution neutron-diffraction experiments have removed many of the anomalies in the structure of Ba_2LaRuO_6

TABLE V

CELL PARAMETERS FOR Ba_2LaRuO_6 AND Ca_2LaRuO_6 AT 2K

	a	*b*	*c*	α	β	γ
Ba_2LaRuO_6	6.0087(3)	6.0537(3)	8.5417(5)	90.54(1)	90.37(1)	89.75(1)
Ca_2LaRuO_6	5.6055(1)	5.8374(1)	8.0526(2)	90	90.25(1)	90

TABLE VI

ATOMIC POSITIONS FOR Ba_2LaRuO_6 AT 2K

Atom	x	y	z
Ba	0.499(1)	0.498(1)	0.2516(8)
La	0	0.5	0
Ru	0.5	0	0
O(1)	0.296(1)	0.246(1)	−0.0294(8)
O(2)	0.246(1)	0.797(1)	0.001(1)
O(3)	0.479(1)	0.036(1)	0.2268(9)

Note. Overall isotropic temperature factor B = 0.56(2) Å^2. Final weighted profile R factor = 8.9%.

deduced previously (*3*); in particular, the bond lengths and bond angles presented in Table II show that the RuO_6 octahedra are more regular than the earlier work suggested. The Ru–O bond lengths lie between 1.93 and 1.99 Å and the O–O distances only vary between 2.73 and 2.80 Å (2.66 and 3.01 Å previously). However, the LaO_6 octahedra are less regular, with O–O distances between 3.23 and 3.37 Å, and the average La–O distance of 2.34 Å is again shorter than that predicted by Shannon and Prewitt (*8*). The Ba–O bond lengths around the A site vary from 2.83 to 3.23 Å with an average of 3.03 Å, in good agreement with Shannon and Prewitt's prediction of 3 Å.

The RuO_6 octahedra in Ca_2LaRuO_6 are very similar in size to those found in Ba_2LaRuO_6, having a range of Ru–O bond lengths of 1.95–1.97 Å and O–O distances between 2.74 and 2.79 Å. The average value of the

TABLE VII

ATOMIC POSITIONS FOR Ca_2LaRuO_6 AT 2K

Atom	x	y	z
Ca/La (*A* site)	0.5136(3)	0.5564(2)	0.2512(4)
Ru	0.5	0	0
Ca	0	0.5	0
O(1)	0.2171(4)	0.1804(4)	−0.0504(3)
O(2)	0.3247(4)	0.7207(4)	−0.0618(3)
O(3)	0.3945(4)	−0.0430(3)	0.2290(3)

Note. Overall isotropic temperature factor B = 0.48(2) Å^2. Final weighted profile R factor = 9.2%

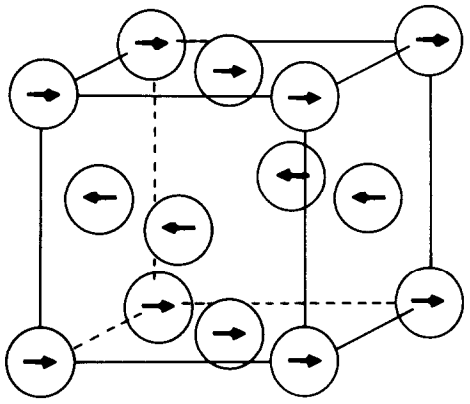

FIG. 5. The Type I magnetic unit cell of Ca_2LaRuO_6. Only ruthenium ions are shown.

Ru–O bond lengths in the two materials is 1.96 Å, which leads to an ionic radius of 0.56 Å for Ru^{5+} in octahedral coordination. The average B-site Ca–O bond length of 2.27 Å is shorter than the predicted value (*8*) of 2.4 Å, and the O–O bond lengths in the CaO_6 octahedra vary between 3.12 and 3.31 Å. Thus in both materials we find regular RuO_6 octahedra and distorted BO_6 octahedra (B = La or Ca) with B–O bond lengths too short to be accounted for within the ionic model.

2. *Magnetic Structures*

Figures 4 and 5 show how the Ru^{5+} ions in Ca_2LaRuO_6 and Ba_2LaRuO_6 form a face-centered array when described in a pseudo-cubic unit cell with a cell parameter ~8 Å. The relative strengths of the two dominant magnetic interactions in such a structure, those between nearest neighbors and those between next-nearest neighbors, determine the type of magnetic ordering found at low temperatures (*9*). In the present discussion of ions with a $4d^3$ electron configuration, we can assume that all the interactions will be inherently antiferromagnetic since they are all between half-filled t_{2g} orbitals. If the 180° next-nearest-neighbor superexchange interaction along the pathway Ru–O–M–O–Ru is dominant, we would expect

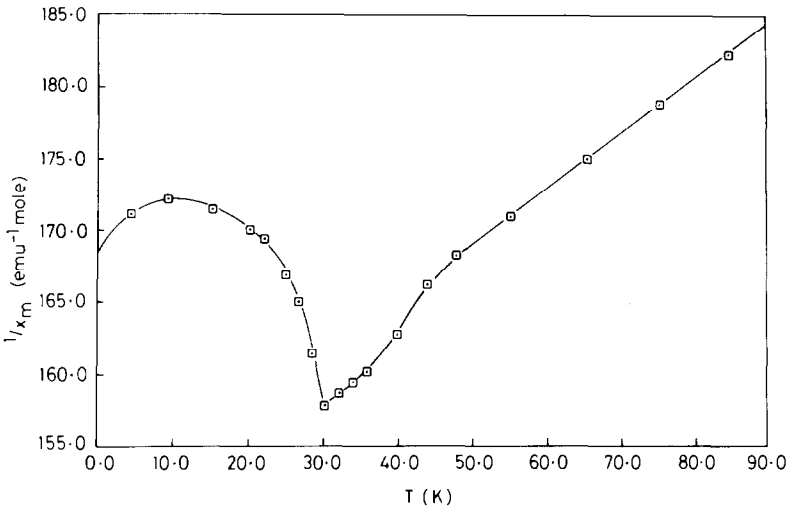

FIG. 6. The reciprocal molar magnetic susceptibility of Ba_2LaRuO_6 as a function of temperature.

to observe Type II ordering (*9*) with each ruthenium ion having all six next-nearest neighbors antiparallel as in MnO. In this collinear-spin case, the only stabilization of the nearest-neighbor interaction occurs via exchange striction since six of the nearest-neighbor spins are parallel and the other six are antiparallel to the central ion. As the relative strength of the nearest-neighbor interaction increases, a collinear-spin configuration moves to Type IIIa ordering in which each ruthenium is antiferromagnetically coupled to eight out of the twelve nearest-neighbor ions while retaining antiparallel alignment with two next-nearest neighbors. Type I ordering is similar to Type IIIa in that eight nearest neighbors are antiferromagnetically coupled to the central ion, but the next-nearest neighbors are all ferromagnetically coupled. Clearly, this pattern of ordering can only occur as the strength of the Ru–O–*M*–O–Ru superexchange approaches zero.

Earlier discussions (*2*) of the magnetic properties of Ba_2LaRuO_6 and Ca_2LaRuO_6 have assumed that both adopt Type II magnetic structures. However, our neutron-diffraction experiments indicate otherwise, with Ba_2LaRuO_6 showing Type IIIa ordering and Ca_2LaRuO_6 Type I. It thus appears that the superexchange through the O–La–O linkages is weak and that through the O–Ca–O linkages it is vanishingly small. Whatever the nature of the intermediate cation, the next-nearest-neighbor superexchange will be relatively weak for a $t_{2g}^3 e_g^0$ electron configuration because the interaction can only take place through the π-orbital system. In the case of La^{3+} ions, which have energetically accessible $5d$ orbitals, the π-bond interaction is weak, but not negligible. In the case of Ca^{2+} ions, the empty $4p_\pi$ orbitals are not energetically accessible, which is why coupling through an O–Ca–O linkage is negligible.

On the other hand, the π-orbital interactions are quite suitable for the nearest-neighbor superexchange interactions, which utilize oxygen $2p_\pi$ orbitals along a Ru–O–O–Ru pathway. Hence the relative strength of the nearest-neighbor interactions can be readily rationalized. Significantly, the magnetic order is not consistent with an important third-nearest-neighbor Ru–A–Ru interaction.

The magnitude of the ordered magnetic

moment is considerably reduced from the spin-only value in both Ba_2LaRuO_6 and Ca_2LaRuO_6. This is to be expected because the covalency in the Ru–O bonds will cause a transfer of spin away from the Ru^{5+} ions. There have been many studies of this effect in compounds of the first transition series (*10*), but none on those of the second series. Hubbard and Marshall (*11*) have used molecular-orbital theory to describe the effects of covalency. From their work we can derive the covalency parameter A_π^2 defined by the equation

$$S/S_0 = 1 - 4A_\pi^2,$$

where S is the observed spin and S_0 is the free-ion spin corrected for zero-point spin deviations. Using the correction calculated by Davis (*12*), we find the following values for A_π^2:

Ba_2LaRuO_6 $8.2 \pm 1\%$,
Ca_2LaRuO_6 $8.6 \pm 1\%$.

These values can be compared to that of 1.6% found for Cr^{3+} in $LaCrO_3$ by Tofield and Fender (*13*). The coefficients for 4*d* orbitals at the smaller, more highly charged Ru^{5+} ions are predictably larger.

3. *Interpretation*

It is instructive to locate Ba_2LaRuO_6 and Ca_2LaRuO_6 on the *T*–*b* phase diagram for half-filled orbitals (*14*) shown in Fig. 7. In this diagram, the Néel temperature T_N and the superconducting transition temperature T_{cs} are plotted schematically against the transfer energy b of tight-binding theory for like transition-metal ions; b is a theoretical measure of the strength of the interatomic interactions. Implicit in the diagram is the intraatomic electron–electron electrostatic interaction-energy U that splits a d^n from a d^{n+1} configuration. In the domain $b < b_c$ where the perturbation energy $\sim b^2/U$ is small enough for the superexchange perturbation expansions to converge, $T_N \sim b^2/kU$ increases monotonically with b. In this domain, crystal-field theory modified by superexchange theory provides an adequate description of the transition-metal d electrons. In the domain $b > b_c$, it is necessary to employ an itinerant-electron description of the electrons. In the range $b_c < b < b_m$, the energy U makes electron correlations among the itinerant electrons strong enough to induce spontaneous magnetism; U is generally large enough, in the case of

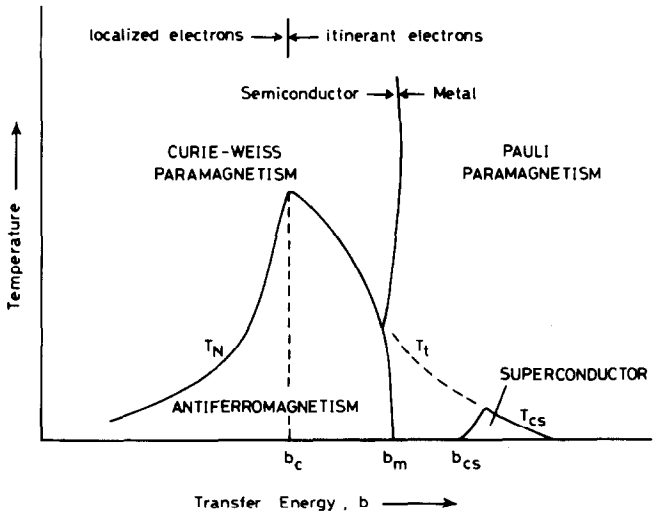

FIG. 7. Conceptual temperature–transfer integral phase diagram for one electron per orbital.

half-filled bands, to also split the bands in two—$w_b \simeq 2zb < U$, where z = number of nearest neighbors—to render the stoichiometric compound semiconducting (provided the Fermi energy does not intersect any overlapping bands). In the range $b > b_m$, the intraatomic energy U responsible for spontaneous magnetism becomes more and more reduced by "screening" with increasing b. However, U remains large enough to quench any transition to the superconducting state in the narrow range $b_m < b < b_{cs}$; in this range the bands may yet be narrow enough for the stabilization of a charge-density-wave (CDW) or spin-density-wave (SDW) state below a transition temperature T_t. In the range $b > b_{cs}$, a superconducting state is stabilized at lowest temperatures; the transition temperature falls with increasing b due to a decrease in density of states at the Fermi energy as described by the Bardeen–Cooper–Schrieffer theory.

In the region $b < b_m$ of strong electron correlations $U > w_b$, the paramagnetic susceptibility for a half-filled band obeys a Curie–Weiss law with Curie constant close to the spin-only value: the molecular Curie constant $C \simeq S_0(S_0 + 1)/2$, where S_0 is the localized-configuration spin, is not complicated by an orbital contribution in first-order theory. However, as b increases to b_m, the high-temperature range in which the Curie law provides a reliable measure of the free-complex S_0 becomes more removed from T_N, and the effective Curie constant $C_{eff} > C$ measured at normal temperatures gives an effective spin S that is too large. Moreover, the measured Weiss constant θ_a no longer bears a simple relation to the Néel temperature T_N in terms of the magnetic order and intrasublattice interaction energy (*9*); the ratio $|\theta_a|/T_N$ becomes anomalously large. On the other hand, the atomic moment μ_A in the antiferromagnetically ordered state, as measured by neutron diffraction, becomes more and more reduced by interatomic charge transfer as b increases to b_m. Therefore, a particularly marked discrepancy appears, as b increases to b_m, in the effective atomic spins S determined from $\mu_A \simeq 2S\mu_B$ by low-temperature neutron diffraction and from $\mu_{eff} \simeq \sqrt{8C}\mu_B \simeq 2\sqrt{S(S+1)}\mu_B$ by the temperature dependence of the inverse paramagnetic susceptibility (χ_m^{-1} vs T). The domain $b_m < b < b_{cs}$ is characterized by a paramagnetic susceptibility that contains an increasing temperature-independent component with increasing b, the magnitude of this component also decreasing until the small, temperature-independent susceptibility of unenhanced Pauli paramagnetism is observed (*15*).

The diagram of Fig. 7 is applicable to Ba_2LaRuO_6 and Ca_2LaRuO_6 because the Ru^{5+}:$4t_{2g}^3e_g^0$ configuration of a free $(RuO_6)^{7-}$ complex offers half-filled orbitals of $4t_{2g}$ parentage that are split from the empty orbitals of $4e_g$ parentage by a large, cubic crystalline field. The orbitally threefold-degenerate Ru manifold of t_{2g} orbitals strongly overlaps the anion p_π orbitals, but not the p_σ orbitals, of a $(RuO_6)^{7-}$ complex. Therefore the ligand-field orbitals of t_{2g} parentage for a complex become

$$\psi_t^* = N_\pi(f_t - \lambda_\pi\phi_\pi),$$

where f_t is the free-cation $4d$ wavefunction of t_{2g} symmetry and ϕ_π is the complex-symmetrized anionic p_π configuration of t_{2g} symmetry admixing with f_t to produce the antibonding ψ_t^* orbital with covalent-mixing parameter λ_π. The large $\lambda_\pi \sim 2A_\pi$ measured indicates a relatively small electrostatic energy U for the correlation splitting between $4t_{2g}^3$ and $4t_{2g}^4$ configurations and a significant transfer energy b for the nearest-neighbor Ru–O–O–Ru intercomplex interactions. Nevertheless, the existence of spontaneous magnetism indicates a $U > w_b \simeq 2zb$ with $b < b_m$. On the other hand, a ruthenium atomic moment $\mu_{Ru} < 2\mu_B$ obtained from neutron diffraction is strongly

reduced from the free-ion spin-only value of $3\mu_B$ for a $4t_{2g}^3$ configuration; this result implies a large superexchange charge transfer between antiferromagnetically coupled Ru^{5+} ions as well as a $4d^3$ form factor that has been contracted by covalent mixing with the nearest-neighbor anions. Such a large reduction in μ_{Ru} implies a $b_c < b < b_m$, and we therefore predict, from Fig. 7, a $dT_N/dP = (\partial T_N/\partial b)(\partial b/\partial P) < 0$ since a $\partial b/\partial P > 0$ is unambiguous for a hydrostatic pressure P.

From the above discussion, it follows that the zero-order problem reduces to a consideration of the half-filled π^* band of a face-centered-cubic $(RuO_6)^{7-}$-complex array, the π^*-band orbitals being derived from the ψ_i^* orbitals. These orbitals are directed toward nearest-neighbor complexes across the face of the pseudocubic perovskite unit cell; and where the nearest-neighbor Ru–O–O–Ru interactions are dominant, the low-temperature magnetic order will optimize antiferromagnetic coupling between nearest neighbors. With a collinear-spin configuration, the constraint of long-range order permits only eight antiparallel-spin nearest neighbors; four nearest neighbors are forced to have parallel spins. This constraint is satisfied for Type I and Type IIIa ordering, but not for Type II ordering. Moreover, Type IIIa ordering optimizes any antiparallel-spin coupling between next-nearest neighbors given dominant nearest-neighbor interactions, whereas Type I order implies either ferromagnetic or negligible next-nearest-neighbor interactions. We pointed out above that the Ru–O–Ca–O–Ru next-nearest-neighbor interactions in Ca_2LaRuO_6 would be negligibly small.

Additional evidence for a nearest-neighbor Ru–O–O–Ru transfer energy b in the range $b_c < b < b_m$ comes from the susceptibility data (*2*), which shows $|\theta_a|/T_N$ values of 13 and 10, respectively. This is quite outside the acceptable limit predicted from a superexchange model (*9*). Moreover, the measured effective magnetic moments are $\mu_{eff} = 4.27\mu_B$ and $4.00\mu_B$, both larger than the spin-only value of $3.87\mu_B$. For a $^4A_{1g}$ ground state, only second-order orbital contributions can be invoked, and these contributions should reduce, not enhance, μ_{eff} relative to its spin-only value. The increase in the measured Curie constant C can, on the other hand, be satisfactorily accounted for if b is close enough to b_m in the range $b_c < b < b_m$ to cause the predicted discrepancy in the effective spins obtained from μ_A and μ_{eff}.

Finally, it also follows from Fig. 7 that T_N should be higher in the compound with the smaller transfer energy b so long as $b_c < b < b_m$. This reasoning implies that Ba_2LaRuO_6, with $T_N = 29.5$K, has a narrower π^* band than Ca_2LaRuO_6 with $T_N = 12$K, which is consistent with the smaller A_π^2 values found for Ba_2LaRuO_6. The smaller covalent mixing in the Ba compound would seem to be contrary to a smaller competition for the anion p_π orbitals by the more basic Ba^{2+} ions; however, the $5d$ orbitals of the B-site La^{3+} ions do introduce an important competition in the Ba compound; the La^{3+} ions only occupy the larger A-site positions in the Ca compounds and may not compete there so strongly.

4. Extension to $CaRuO_3$ and $SrRuO_3$

These findings for Ba_2LaRuO_6 and Ca_2LaRuO_6 are significant because they provide the first firm evidence that M–O–O–M interactions across the face of a pseudocubic perovskite cell may, in the case of $4d$ orbitals on a transition-metal cation of high valence, be strong enough to make any $4d$ electrons become itinerant, even if strongly correlated. Given this finding, it is interesting to return to the magnetic properties of the perovskites $CaRuO_3$ and $SrRuO_3$ containing low-spin Ru^{4+}: $4t_{2g}^4e_g^0$ configurations. Here the Ru(IV)–O–Ru(IV) interactions are strong enough

to produce itinerant-electron π^* bands, but again U is large enough to induce strong correlations with a magnetic susceptibility obeying a well-behaved Curie–Weiss law. Moreover, $SrRuO_3$ is a metallic ferromagnet with a $\mu_{Ru} \simeq 1\mu_B$, consistent with itinerant-electron ferromagnetism in a narrow π^* band having $b_c < b < b_m$ and a spontaneous magnetism following a Slater–Pauling curve (*16*). The compound $CaRuO_3$, on the other hand, has a negative Weiss constant, suggesting antiferromagnetic order, but Mössbauer data (*17*) indicate there is no long-range magnetic order at 4K. Since the π^* bands in $CaRuO_3$ can be expected to be narrower, competition for the p_π orbitals being stronger from Ca^{2+} than Sr^{2+} ions, this lack of spontaneous magnetism in a material with a well-behaved Curie–Weiss law for the paramagnetic susceptibility must be considered remarkable. It has been argued (*14*) that a change from spontaneous ferromagnetism to spontaneous antiferromagnetism would occur in a band two-thirds filled at that bandwidth where $\mu_F \simeq \mu_{AF}$, the stable magnetic phase being the one that stabilized the highest atomic moment (*14*). The ferromagnetic moment $\mu_F = 1\mu_B$ is predicted unambiguously from theory; the antiferromagnetic moment $\mu_{AF} = (2 - \delta)\mu_B$ depends upon the bandwidth through the charge-transfer reduction factor δ. We have seen that a $\delta > 1$ is found in Ba_2LaRuO_6 and Ca_2LaRuO_6, and we can anticipate a similar reduction in $CaRuO_3$ and $SrRuO_3$. Therefore a $\mu_F > \mu_{AF}$ in $SrRuO_3$ and a $\mu_F < \mu_{AF}$ in $CaRuO_3$ would be qualitatively reasonable and consistent with a narrower π^* band in $CaRuO_3$. Hence the paramagnetic data are reasonable and consistent. What is peculiar, then, is the lack of any long-range magnetic order in $CaRuO_3$. The inescapable implication is that where $\mu_F \simeq \mu_{AF}$, the system is magnetically unstable with respect to long-range magnetic order. Such a conclusion deserves further study.

Acknowledgments

We are grateful to Alan Hewat and Steve Heathman for their help at ILL Grenoble. One of us (P.D.B.) is supported as a Research Fellow at St. Catherine's College, Oxford, by the Central Electricity Generating Board. The neutron diffraction data were analyzed using the SERC Interactive Computing Facility (Grant GR/B/52151).

References

1. P. C. DONOHUE AND E. L. MCCANN, *Mater. Res. Bull.* **12,** 519 (1977).
2. R. Greatrex, N. N. Greenwood, M. Lal, and I. Fernandez, *J. Solid State Chem.* **30,** 137 (1979).
3. P. D. BATTLE, *Mater. Res. Bull.* **16,** 397 (1981).
4. H. M. RIETVELD, *J. Appl. Crystallogr.* **2,** 65 (1969).
5. A. K. CHEETHAM AND J. C. TAYLOR, *J. Solid State Chem.* **21,** 253 (1977).
6. G. E. BACON, "Neutron Diffraction," 3rd ed., Oxford Univ. Press, (Clarendon), Oxford (1975).
7. R. A. TAHIR-KHELI, H. B. CALLEN, AND H. JARRETT, *J. Phys. Chem. Solids* **27,** 23 (1966).
8. R. D. SHANNON AND C. T. PREWITT, *Acta Crystallogr. Sect. B* **25,** 925 (1969).
9. J. B. GOODENOUGH, "Magnetism and the Chemical Bond," Wiley, New York (1963).
10. B. C. TOFIELD, *J. Phys. Colloq. C* **6,** 539 (1976).
11. J. HUBBARD AND W. MARSHALL, *Proc. Phys. Soc.* **86,** 561 (1965).
12. H. H. DAVIS, *Phys. Rev.* **120,** 789 (1960).
13. B. C. TOFIELD AND B. E. F. FENDER, *J. Phys. Chem. Solids* **31,** 2741 (1970).
14. J. B. GOODENOUGH, *in* "Magnetism in Metals and Metallic Compounds" (J. T. Lopusanski, A. Pekalski, and J. Przystawa, Eds.), p. 35, Plenum, New York (1976).
15. J. B. GOODENOUGH, "Proceedings, 14th Robert A. Welch Foundation Conference on Chemical Research," p. 75 (1970).
16. J. M. LONGO, P. M. RACCACH, AND J. B. GOODENOUGH, *J. Appl. Phys.* **39,** 1327 (1968).
17. T. C. GIBB, R. GREATREX, N. N. GREENWOOD, AND P. KASPI, *J. Chem. Soc. Dalton,* 1253 (1973).